Cerebral Cortex July 2014;24:1806–1817
doi:10.1093/cercor/bht030
Advance Access publication February 8, 2013

Spatiotemporal Dependency of Age-Related Changes in Brain Signal Variability

A. R. McIntosh[1], V. Vakorin[1], N. Kovacevic[1], H. Wang[1], A. Diaconescu[2] and A. B. Protzner[3]

[1]Rotman Research Institute of Baycrest, Canada, [2]Institute for Empirical Research in Economics, University of Zurich, Switzerland and [3]Department of Psychology, University of Calgary, Canada

Address correspondence to A. R. McIntosh, Rotman Research Institute of Baycrest Centre, 3560 Bathurst Street, Toronto, Ontario M6A 2E1, Canada. Email: rmcintosh@research.baycrest.org

Recent theoretical and empirical work has focused on the variability of network dynamics in maturation. Such variability seems to reflect the spontaneous formation and dissolution of different functional networks. We sought to extend these observations into healthy aging. Two different data sets, one EEG (total $n = 48$, ages 18–72) and one magnetoencephalography ($n = 31$, ages 20–75) were analyzed for such spatiotemporal dependency using multiscale entropy (MSE) from regional brain sources. In both data sets, the changes in MSE were timescale dependent, with higher entropy at fine scales and lower at more coarse scales with greater age. The signals were parsed further into local entropy, related to information processed within a regional source, and distributed entropy (information shared between two sources, i.e., functional connectivity). Local entropy increased for most regions, whereas the dominant change in distributed entropy was age-related reductions across hemispheres. These data further the understanding of changes in brain signal variability across the lifespan, suggesting an inverted U-shaped curve, but with an important qualifier. Unlike earlier in maturation, where the changes are more widespread, changes in adulthood show strong spatiotemporal dependence.

Keywords: electroencephalograpy, functional connectivity, magnetoencephalography, multiscale entropy, nonlinear dynamics

Introduction

It is becoming clear that brain signal variability (i.e., transient temporal fluctuations in brain signal) conveys important information about network dynamics (Deco et al. 2011). In neural network modeling, information integration across widespread neural networks is achieved through the emergence and disappearance of correlated activity between brain regions over time and across multiple timescales (Jirsa and Kelso 2000; Honey et al. 2007). Such transient changes cause fluctuations in the temporal dynamics of the corresponding brain signal; networks with more potential configurations elicit a more variable response. In turn, signal variability may represent the information processing capacity of the system, where higher variability reflects greater information integration across the network.

Our empirical studies have noted developmental increases of brain signal variability that could be related to the idea that variability reflects the capacity for information processing. The first study (McIntosh et al. 2008) examined EEG signal variability using two measures; (1) principal components analysis (PCA) of single trial data, where a more variable brain would produce a greater number of principal components, and (2) multiscale entropy (MSE), a measure that is sensitive to linear and nonlinear variability and is able to differentiate variability of a complex system such as the brain, from a purely random system (Costa et al. 2002; Costa et al. 2005). Both PCA and MSE analyses indicated that EEG signal variance increased from ages 8 to 15 and was even higher in young adults. Furthermore, behavioral stability (measured by accuracy and intra-subject variability of reaction time) was greater with a more variable brain signal, suggesting that a more variable brain produces more stable behavior. Misic et al. (2010) replicated this finding across a slightly wider age range (6–16 years) and using magnetoencephalography (MEG). Finally, Lippe et al. (Lippe et al. 2009) extended these observations to infants, showing that EEG signal complexity increased from 1 month to 5 years in response to auditory and visual stimuli. Interestingly, the trajectories of the change were not the same for the auditory and visual responses, in that auditory responses were more complex than visual in infants and complexity in both modalities gradually merged to be indistinguishable in adults.

During maturation from childhood to adulthood, the brain becomes more specialized in that a larger repertoire of individualized physiological states for separate brain regions develops. Integration between distributed neuronal populations also increases. Vakorin et al. (Vakorin et al. 2011) introduced a method to decompose the total variability of signals into local entropy that characterizes the dynamics within brain areas and distributed entropy that characterizes the signal variability attributed to information exchange between areas. Using these measures, the present study explored the interplay between specialization and integration and how these factors contribute to changes in brain complexity in development. The results suggested that increased integration was the key factor contributing to the developmental increase in complexity of brain signals. Specifically, developmental changes were characterized by a decrease in the amount of information processed locally, accompanied by an increase in distributed entropy.

The structural and functional changes during adult aging are less global than those during early maturation. Extant literature has characterized more heterogeneous changes in structure, with areas showing different rates of change with age (Guttmann et al. 1998; Courchesne et al. 2000; Raz and Rodrigue 2006). Similarly, functional networks seem to show different rates of change that seem to reflect changes in the cognitive functions they support (Grady 1998; Greenwood 2000; Grady et al. 2003; Andrews-Hanna et al. 2007; Damoiseaux et al. 2007; Park and Reuter-Lorenz 2009). If we consider such alterations in the context of nonlinear systems, one may predict that brain signal variability should also show changes, but perhaps less globally than was observed for children. Indeed some of our work with functional MRI suggests both regional increases and decreases of variability in normal aging (Garrett et al. 2011; Garrett et al. 2012).

Our measures of brain signal variability can be most readily appreciated from the perspective of complex systems. Compared with deterministic or random systems, complex systems such as the brain have a greater capacity for information processing (Tononi et al. 1994; Sporns et al. 2000a; Sporns et al. 2000b). Entropy measures are sensitive to the information content in signals, and thus the measures of MSE, distributed and local entropy, are estimates of the information and so too, complexity. Thus, we can reframe the focus of the study as follows: development brings with it the evolution of a brain that has greater capacity for information processing. Whereas this evolution likely continues into early adulthood, it is less clear how the trend changes in senescence. A handful of studies that have measured complexity of EEG in aging have produced conflicting results (e.g., Anokhin et al. 1996; Pierce et al. 2000; Gaal et al. 2010). Thus, a key aspect of our current work is to characterize the different temporal scales over which information integration may take place in the brain. Although we found that information processing capacity increases across most scales in development, given that changes in late adulthood are not as global as they are early in life, it is likely that the characterization of changes in information processing capacity will depend on spatiotemporal scale.

We sought to characterize the changes in brain signal variability across two different adult samples from two studies. One study tested adults from 19 to 72 years and measured EEG in a range of visual perception tasks. The second study tested adults from 20 to 75, with no participants in the middle-age range and examined MEG response in a multisensory task (Diaconescu et al. 2012). For both data sets, analysis was done based on cortical source solutions rather than in original sensor space to increase the spatial location precision, given the spatial differences reported for age-related changes and to minimize the artifact of volume conduction for analyses of functional connectivity (Srinivasan et al. 1998). The purpose of the present work was to get general characterizations of age-related changes in variability to see how they complement those we observed early in development.

Methods

The study was based on the analysis of two different data sets. Both focused on the age-related changes in evoked activity to sensory stimuli. Both studies were approved by the joint Baycrest Centre–University of Toronto Research Ethics Committee, and the rights and privacy of the participants were observed. All participants gave formal informed consent before the experiment and received monetary compensation.

Study 1—EEG

Sixteen young adults (6 males, mean age 22 ± 3 years), 16 middle-age adults (7 males, mean age 45 ± 6 years), and 16 older adults (5 males, mean age 66 ± 6 years) participated in the EEG study. All participants had healthy neurological histories, and normal or corrected-to-normal vision.

Apparatus and Task

EEG recordings from 76 electrodes were collected using BioSemi Active Two system with a bandwidth 99.84 (0.16–100) Hz and sampling rate of 512 Hz. Data were recorded reference free, but were converted to an average reference at Cz during the pre-processing.

The EEG data were part of a larger study that contained six different conditions (similar to the configuration of tasks used in a fMRI study by Grady et al. (2010)). For the purposes of the present work, we used two tasks, visual perceptual matching (PM) and delayed-match-to-sample (DMS). Presentation (version 10.3, Neurobehavioural Systems, Inc.) and Matlab (version 7, Mathworks) were used to control visual stimulus delivery and to record participants' response latency and accuracy. Stimuli were one-dimensional Gaussian white noise fields with a two-octave frequency filter and were presented simultaneously in a triangular array. In the PM task, subjects indicated which of the three bottom stimuli matched the one on the top by pressing one of three buttons. The task instructions for DMS were the same as for PM, except that in DMS, the top row stimulus appeared first for 1.5–2 s and then disappeared before the bottom row stimuli were shown. There was a 4-s delay between the onsets of top (encoding phase) and bottom stimuli (recognition phase). For the present study, only the data from PM and the encoding phase of DMS were used.

We used a psychophysical thresholding procedure to ensure that subjects were matched in terms of accuracy by adjusting stimulus discriminability so that each person was 80% accurate (Protzner and McIntosh 2007). Stimulus discriminability was manipulated by modifying the center frequency ratio. For example, at a ratio of 2, and a base frequency of 2 c/deg, the center frequencies were 2 c/deg, 4c/deg, and 8c/deg. To decrease stimulus discriminability, a ratio of 1.5 would produce center frequencies of 2 c/deg, 3 c/deg, and 4.5 c/deg.

Data Pre-processing

Continuous EEG recordings were bandpass filtered from 0.5 to 55 Hz. Only trials with correct responses were analyzed. Data were epoched and base-lined into 500-2000 ms epochs with a 500-ms pre-stimulus baseline. Artifact removal was performed using independent component analysis in EEGLAB (Delorme and Makeig 2004). There was an average of 182 trials for the PM task and 171 for the DMS task after data processing was completed for all subjects. There was no significant difference in the number of useful trials between conditions or groups.

To further localize the dynamics of source activity at specific locations, we identified 72 ROI's in Talairach space (Diaconescu et al. 2011) and performed source estimation at these locations using sLORETA (Pascual-Marqui 2002), as implemented in Brainstorm (Tadel et al. 2011), which is documented and freely available for download under the GNU general public license (http://neuroimage.usc.edu/brainstorm). Source reconstruction was constrained to the cortical mantle of a brain template MNI/Colin27 defined by the Montreal Neurological Institute. Current density for three source orientations (X, Y, and Z components) was mapped at 72 brain regions of interest adapting the regional map coarse parcellation scheme, as developed in Kotter and Wanke (2005) (see Table 1). For each subject, MSE measures of source waveforms were calculated for the PM task and the encoding part of the DMS task.

Study 2—MEG Data

Fifteen young adults (7 males, mean age 23 ± 3 years) and 16 older adults (8 males, mean age 70 ± 5 years) with an average of 16.5 years of education participated. All participants were right handed with healthy neurological histories, and normal to corrected-to-normal vision. All participants were audiometrically screened to determine hearing thresholds for each ear separately; adults whose hearing thresholds exceeded 15dB hearing level were excluded from participation, as that was considered below normal levels. The young adults who participated in the study had average hearing thresholds of 2 dB (range 0–8 dB), and older adults had average hearing thresholds of 10 dB (range 5–15 dB).

Apparatus and Task

Auditory and visual stimuli were used in this study. Black and white line drawings selected from a database (Snodgrass and Vanderwart 1980) were used for visual presentations. All visual stimuli were matched according to size (in pixels), brightness, and contrast. Auditory stimuli were selected from a local database of non-speech, complex sounds (e.g., animal calls, car horns). Complex sounds were matched according to amplitude. Complex sounds were delivered

Table 1
Regional map coordinates with reference to the Talairach–Tournoux Atlas

x	*y*	*z*	Region	Short name
0	32	24	Anterior cingulate cortex	CCA
0	−32	24	Posterior cingulate cortex	CCP
0	−48	12	Retrosplenial cingulate cortex	CCR
0	16	−8	Subgenual cingulate cortex	CCS
40	−14	4	A1	A1
60	−14	4	A2	A2
36	8	56	Frontal eye fields	FEF
36	16	−4	Anterior insula	IA
36	−8	−4	Claustrum	IP
24	−24	56	M1	M1
44	−48	20	Inferior parietal cortex	PCI
44	−64	28	Angular gyrus	PCIP
8	−64	54	Precuneus	PCM
8	−64	54	Superior parietal cortex	PCS
48	32	12	Centrolateral prefrontal cortex	PFCCL
48	36	32	Dorsolateral prefrontal cortex	PFCDL
8	36	40	Dorsomedial prefrontal cortex	PFCDM
8	48	20	Medial prefrontal cortex	PFCM
24	44	−20	Orbitofrontal cortex	PFCORB
24	64	4	Frontal polar	PFCPOL
48	32	−8	Ventrolateral prefrontal cortex	PFCVL
28	−16	−16	Parahoppocampal cortex	PHC
48	0	60	Dorsolateral premotor cortex	PMCDL
4	0	60	Medial premotor cortex	PMCM
44	4	24	Ventrolateral premotor cortex	PMCVL
16	−28	4	Pulvinar	PULVINAR
40	−28	64	S1	S1
56	−16	16	S2	S2
64	−24	−12	Middle temporal cortex	TCC
64	−24	−24	Inferior temporal cortex	TCI
52	12	−28	Temporal pole	TCPOL
52	−4	−8	Superior temporal cortex	TCS
32	−28	−28	Ventral temporal cortex	TCV
8	−8	4	Thalamus	THALAM
4	−84	−4	V1	V1
4	−96	8	V2	V2
20	−88	20	Cuneus	VACD
20	−84	−12	Fusiform gyrus	VACV

binaurally at an intensity level of 60 dB HL based on the audiometric mean across both ears. There were 40 trials for each condition.

Presentation software (version 10.3, Neurobehavioural Systems, Inc.) was used to control visual and auditory stimulus delivery and to record participants' response latency and accuracy. The time interval between the end of the stimulus presentation and the beginning of the next trial was between 2 and 4 s (equiprobable). Participants were instructed to respond to any trial type, auditory or visual, as quickly as possible with their left index finger response.

The MEG recordings were acquired in a magnetically shielded room at the Rotman Research Institute, Baycrest Centre using a 151-channel whole head neuro-magnetometer (OMEGA, VSM Medtech Inc., Vancouver, Canada). Participants sat in upright position and viewed the visual stimuli on a back projection screen that subtended approximately 30° of visual angle when seated 70 cm from the screen. With regard to the visual presentations, the MEG collection was synchronized to the onset of each stimulus by recording the luminance changes of the screen with a photodiode. Binaural auditory stimuli were presented at 60 dB HL via OB 822 Clinical Audiometer through ER30 transducers (Etymotic Research, Elk Grove, USA) and connected with 1.5 m of length matched plastic tubing and foam earplugs to the participants' ears. With respect to the auditory stimuli, the MEG data collection was synchronized to the onset of the auditory sound envelope.

Neuromagnetic activity was sampled at a rate of 1250 Hz. Third gradient noise correction was applied to the continuous MEG data. Afterward, the MEG data were parsed into epochs including a 200 ms pre- and 1000 ms post-stimulus activity window, and DC offsets were removed from the entire epoch. The data were bandpass filtered between 0.1 and 55 Hz. A principal component analysis was performed on each epoch, and components larger than 2.0 picoTesla (pT) at any time point were subtracted from the data to remove large artifacts caused by eye blinks.

MEG data were co-registered to each participant's individual structural MRI to constrain the sources of activation to each participant's head shape and structural anatomy. MRI scans were acquired for each participant using a 3.0T Siemens Tim MAGNETOM Trio MRI scanner (Software level Syngo MR, Siemens Medical, Germany) with 12-channel head coil.

To obtain spatial precision without integrating power over long temporal windows, we used an event-related version of the synthetic aperture magnetometry analysis technique introduced by Cheyne et al. (2006) to identify evoked brain responses from unaveraged, single trial data. The spatial filter included the same 72 brain regions of interest in Talairach coordinate space as used in the EEG data set (Table 1). The individual functional maps were overlaid on the individual participant's MRI based on co-registration with the indicator coils placed on the nasion and bilateral pre-auricular points. The functional data were then transformed to the standard Talairach–Tournoux space using the same transformation applied to the structural MRI [AFNI software, Cox (1996)].

MultiScale Entropy. Full details of MSE and its relevance for the analysis of signal complexity are given in Costa et al. (2002) and Costa et al. (2005). The utility of MSE for characterizing complexity of brain signals has been confirmed by numerous studies (Bhattacharya et al. 2005; McIntosh et al. 2008; Lippe et al. 2009; Takahashi et al. 2009; Misic et al. 2010; Protzner et al. 2010; Catarino et al. 2011).

To calculate MSE, we used the algorithm available at www.physionet.org/physiotools/mse/ that computes MSE in two steps. First, the algorithm progressively down-samples the EEG post-stimulus time series per trial and per condition (i.e., for timescale t, the coarse-grained time series is constructed by averaging data points within non-overlapping windows of length t). Second, the algorithm calculates the sample entropy for each coarse-grained time series. Sample entropy quantifies the variability of a time series by estimating the predictability of amplitude patterns across a time series. The pattern length was set to $m = 2$; that is, two consecutive data points were used for pattern matching. The similarity criterion was set to $r = 0.5$; data points were considered to have indistinguishable amplitude values (i.e., to 'match") if the absolute amplitude difference between them was ≤5% of the time series standard deviation. For each subject, a source specific MSE estimate was obtained as a mean across single trial entropy measures for each timescale.

Local and Distributed Entropy. The specific derivation of local versus distributed entropy has been described in our previous publication (Vakorin et al. 2011). In information theory (Shannon 1949), entropy $H(X)$ of single random variable X can be defined as a measure of uncertainty associated with X. Conditional entropy $H(X|Y)$ of X given another random variable Y is the entropy of X, provided that the uncertainty about Y is excluded. The reduction in uncertainty due to another variable is called mutual information. Specifically, the mutual information between two random variables X and Y is defined as

$$I(X;Y) = H(X) - H(X|Y). \quad (1)$$

The mutual information is a measure of affiliation between two variables, similar to a correlation coefficient.

The joint entropy $H(X, Y)$, which represents the uncertainty of a pair of random variables (X, Y), can be partitioned into the conditional entropies of the variables X and Y and the mutual information between them. Specifically,

$$H(X,Y) = H(X|Y) + H(Y|X) + I(X;Y). \quad (2)$$

Suppose that a network of M interacting neural sources is identified, and source dynamics are described by M variables Xi, where $i = 1, \ldots, M$. For a given pair of sources, i and j, the information contained in the dynamics of source i can be partitioned into the local entropy associated only with source i and the distributed entropy that is shared between sources i and j. The local entropy corresponds to the conditional entropy $H(Xi|Xj)$. For a given source i, the local entropy, $E_{local}(i)$, can be computed by averaging conditional entropy $H(Xi|Xj)$

over all other sources Xj, $j = i$, constituting the network, whereas the distributed entropy $E_{distrib}(i, j)$ is represented by the mutual information $I(Xi;Xj)$. It should be noted that in practice, however, estimation of information-theoretic measures based on finite noisy time series may be of crucial importance. In this study, we estimated E_{local} and $E_{distrib}$ as described in Vakorin et al. (2011), using the corresponding correlation integral C that is generally considered more accurate than box-counting techniques for calculation of joint entropies (Silverman 1986; Prichard and Theiler 1995).

In addition, we will estimate the local entropy and mutual information on different timescales, based on downsampling of the original time series. Zhang (Zhang 1991) computed the Shannon entropy of time series at various scales that is similar to the approach used for MSE. Downsampling alleviates linear stochastic effects, such as autocorrelation of the brain signals, that might lead to a bias in estimation of the entropy and mutual information (Kaffashi et al. 2008).

PLS Analysis. Partial least squares analysis (PLS McIntosh et al. 1996; McIntosh and Lobaugh 2004; Krishnan et al. 2011) was used to assess age-related changes in spatiotemporal distributions of the entropy measures. Similar to multivariate techniques like canonical correlation analysis, PLS operates on the entire data structure at once, extracting the patterns of maximal covariance between two data

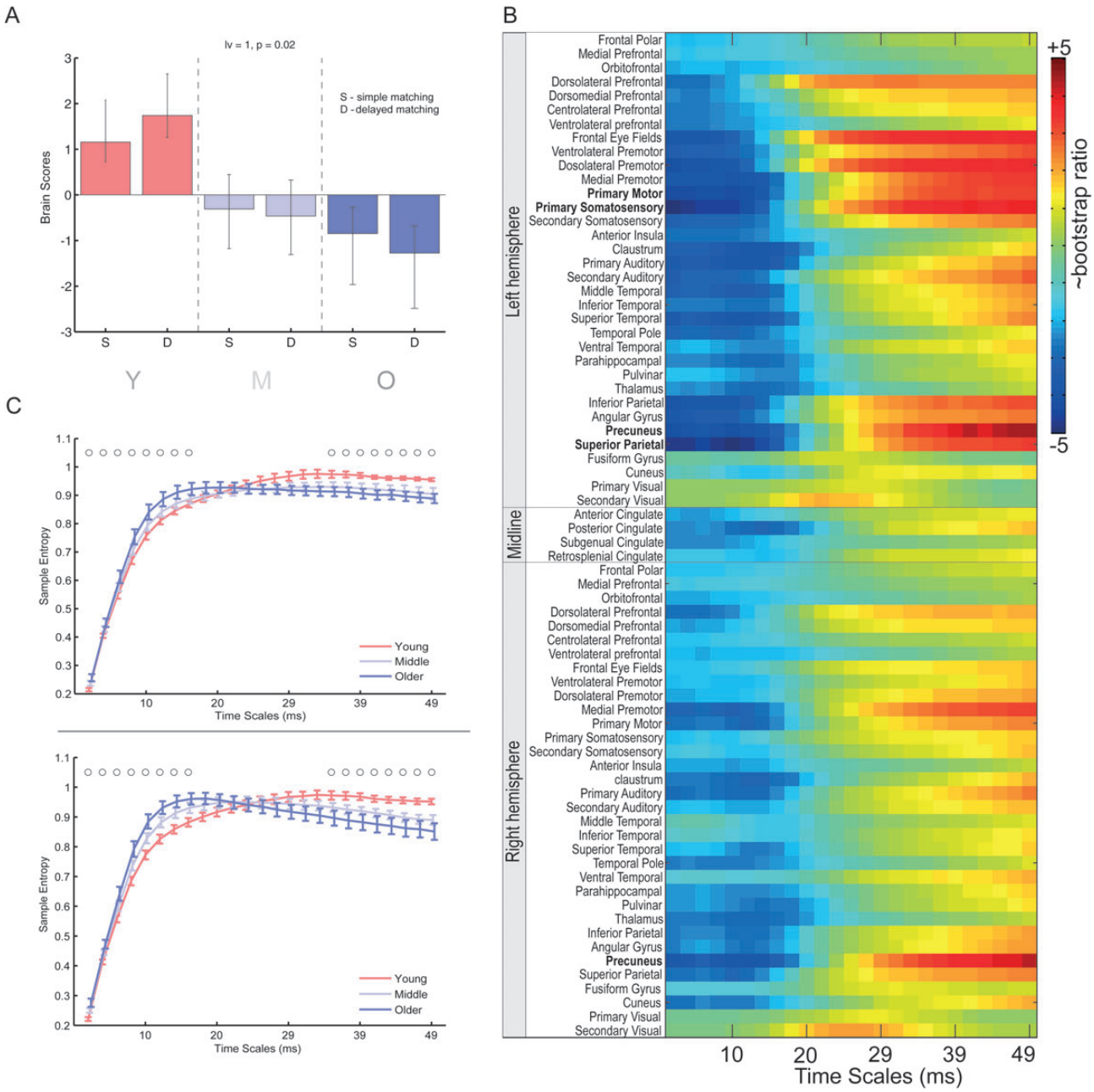

Figure 1. PLS result from the EEG data set for the comparison of age-related changes in MSE. (*A*) The bar graph depicts the data-driven contrast between age groups that was significantly expressed across the entire data set (source × timescales) as determined by permutation tests. (*B*) The statistical image plot represents the regional sources and timescale at which the contrast was most stable as determined by bootstrapping. Values represent the ratio of the parameter estimate for the source divided by the bootstrap-derived standard error (roughly *z* scores). Positive values indicate timescales and sources showing decreased MSE with age and negative values denote age-related increases. Text labels in bold font indicate regions where the bootstrap ratio is greater than 4.0. (*C*) Average MSE (±SE) curves for each group for the regional source in right precuneus for the simple (top) and delayed (bottom) matching tasks. Circle above the curves indicate the timepoints with reliable confidence intervals.

matrices, in the present case group membership (age) and the entropy measures.

Statistical assessment in PLS is done across two levels. First, the overall significance of each pattern, or latent variable (LV), that relates the two data sets is assessed with permutation testing (Good 2000). An LV was considered significant if the observed pattern was present less than 1% of the time in random permutations (e.g., $P < 0.01$). The second level uses bootstrap resampling to estimate confidence intervals around the individual weights in each LV, allowing for an assessment of relative contribution of particular locations and timescales, in the case of the brain side of the equation, and the stability of the relation with age group in the case of the other side of the equation (Efron and Tibshirani 1986; Efron and Tibshirani 1993). For the brain data, we plot bootstrap ratios (ratio of the individual weights over the estimated standard error) as a proxy for the confidence interval. Confidence intervals are plotted for group effects. A minimum threshold of a stable 95% confidence interval was used for all analysis.

Results

Behavior Analysis

EEG Experiment: all groups maintained an accuracy level at or greater than 80% for all tasks, and this level did not differ

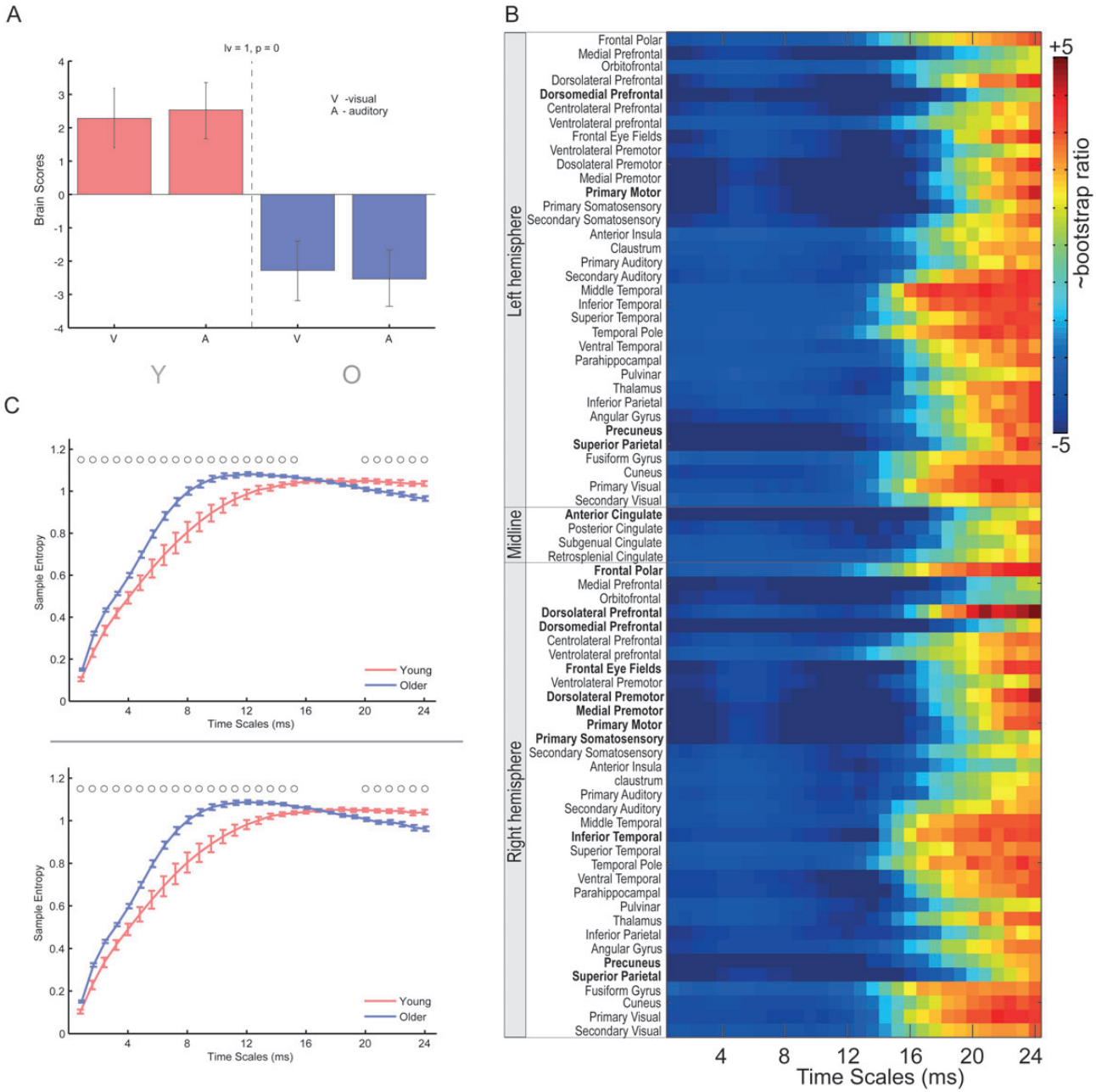

Figure 2. PLS result from the MEG data set for the comparison of age-related changes in MSE. (*A*) The bar graph depicts the data-driven contrast between age groups that was significantly expressed across the entire data set (source × timescales) as determined by permutation tests. (*B*) The statistical image plot represents the regional sources and timescale at which the contrast was most stable as determined by bootstrapping. Values represent the ratio of the parameter estimate for the source divided by the bootstrap-derived standard error (roughly *z* scores). Positive values indicate timescales and sources showing decreased MSE with age and negative values denote age-related increases. Text labels in bold font indicate regions where the bootstrap ratio is greater than 4.0. (*C*) Average MSE (±SE) curves for each group for the regional source in right dorsolateral prefrontal cortex for auditory (top) and visual (bottom). Circle above the curves indicate the timepoints with reliable confidence intervals.

between groups. Mean reaction time was different between groups, showing the typical slowing effect with age (PM: $F(2,45) = 4.14$, $P < 0.05$; DMS: $F(2,45) = 8.92$, $P < 0.01$). There was a slight group difference in the PM task only, with the youngest age group showing more variation than the middle age or oldest group ($F[2,45] = 4.3$, $P < 0.05$).

MEG Experiment: accuracy was above 90% for both groups in the two detection tasks, with the older subjects showing slightly lower accuracy in the visual condition (91 vs. 98%). Mean reaction time was slower in general for older subjects ($F[1,29] = 5.88$, $P < 0.05$), and the coefficient of variation of reaction time was higher in the older group ($F[1,29]$, 12.36, $P < 0.01$).

Aging and MSE

In both data sets, we observed significant changes in MSE distribution with age. There were no reliable interactions of age with task in both data sets. Although we treated age as a categorical grouping factor, the results do not change if age is treated as a continuous measure. Unlike what we have observed in children, this age effect depended on temporal scale.

In the EEG data set, we observed a progressive increase in sample entropy at fine temporal scales with age (Fig. 1*A*), roughly from 2 to 15 ms and then a cross-over at coarse scales with young subjects showing greater sample entropy at approximately 20 ms (Fig. 1, *B,C*). These differences were not homogeneous across source space, with the strongest effects in medial cortical sources such as precuneus and superior parietal lobe (Fig. 1*C*).

For the MEG data set, a similar pattern was observed, although the age differences were much stronger (Fig. 2*A*). At fine scales, the older adults showed greater sample entropy from 2 to 15 ms. The cross-over of the curves took place around 16 ms at which point sample entropy was higher in young adults (Fig. 2*B*, *C*), similar to the EEG data. The effects of fine scale were quite robust across most sources, whereas the difference at coarse scales showed more spatial variation concentrating mainly on temporal and occipital cortical sources (Fig. 2*C*).

Local Versus Distributed Entropy

Local Entropy

For local entropy, PLS analyses revealed the existence of one significant LV in both MEG and EEG data. Specifically, Figure 3 shows the age-related patterns of changes in local entropy for MEG (left column) and EEG (right column). The upper panels in Figure 3*A* and *D* illustrate the corresponding age-related trends of changes in the variability of brain signals associated with the information processed locally.

The overall distributions of the bootstrap values for all sources and timescales are shown in Figure 3*B* and *E*, for MEG and EEG, respectively. Figure 3*C* and *F* shows the same bootstrap ratio values as the function of timescales for all brain sources, each associated with a curve. As can be seen,

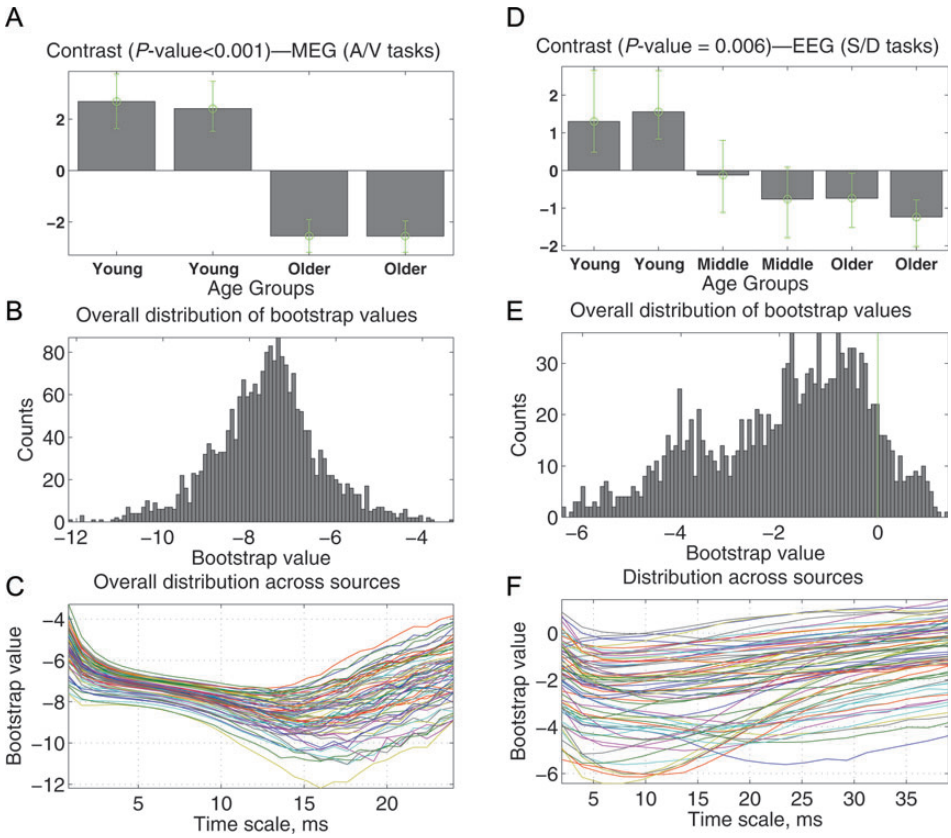

Figure 3. Age-related changes in local entropy: MEG (left) and EEG (right), from the PLS analysis. Panels (*A* and (*D*) illustrate the data-driven contrasts. Expression of these trends is shown in (*B*) and (*E*) as the distributions of all the bootstrap ratio values for all regional sources. The same bootstrap ratio values are plotted in (*C*) and (*F*) as functions of timescales.

the overall distributions of the bootstrap values are significantly skewed toward negative numbers. Considered together with the effect in Figure 3*A* and *D*, this would imply that the dominant effect in aging is an increase of amount of information processed locally.

Distributed Entropy

One significant LV was found both for the EEG and MEG data in the analysis of distributed entropy. The upper panels *A* and *E* in Figure 4 illustrate the corresponding effects (P-value < 0.001 in both cases) underlying the group differences. The corresponding overall distributions of the bootstrap ratio values associated with the pairwise connections between the brain regions and timescales are given in Figure 4*B* and *G*. As can be seen, there are relatively large negative and positive bootstrap ratio values, although the bulk of the connections show positive ratios. In conjunction with the effect in Figure 4*A* and *E*, this would indicate that there are more decreases than increases of distributed entropy in relation to aging. This difference is strongest in the MEG data set.

The difference between decreased and increased distributed entropy is broken down further in Figure 4, which shows how the strength of effects attributed to age-related changes in distributed entropy varies across timescales. Specifically, we identified the 2.5%-tails, cut off by 0.025- and 0.975-quantiles, of the overall distributions of the bootstrap ratio values in Figure 4*B* and *F*. At each timescale, the number of connections with the bootstrap ratio values larger than the 0.975-quantile was computed. These numbers are plotted in Figure 4*C* and *G*. In a similar way, the number of connections with the bootstrap ratio values smaller than the 0.025-quantile is plotted in Figure 4*C* and *G*, as a function of timescale.

Figures 5 and 6 show the spatial patterns supporting the corresponding age-related changes in connectivity between the brain regions. We plotted the bootstrap ratio values at scales around 7 ms for decreased entropy, and 27 ms for increased entropy, for MEG, and around 20 ms (decreased) and 8 ms (increased), for EEG. These time points correspond to the peak distribution of bootstrap by time shown in Figure 4, hence the difference in the peaks between the data sets. The spatial distribution of these changes did not change appreciably across other time points.

Pairwise connections that show decreased entropy with age are depicted in Figure 5. A threshold of >1 was used for the figure to emphasize the spatial distribution. The corresponding lower panels of Figure 5 show the distribution of the bootstrap ratio values associated with local entropy. Similar to Figure 5, Figure 6 shows the distribution of connections showing increased entropy with age.

An obvious spatial pattern is evident in Figures 5 and 6. The networks can be differentiated from the perspective of inter- versus intra-hemispheric connections. As can be seen in

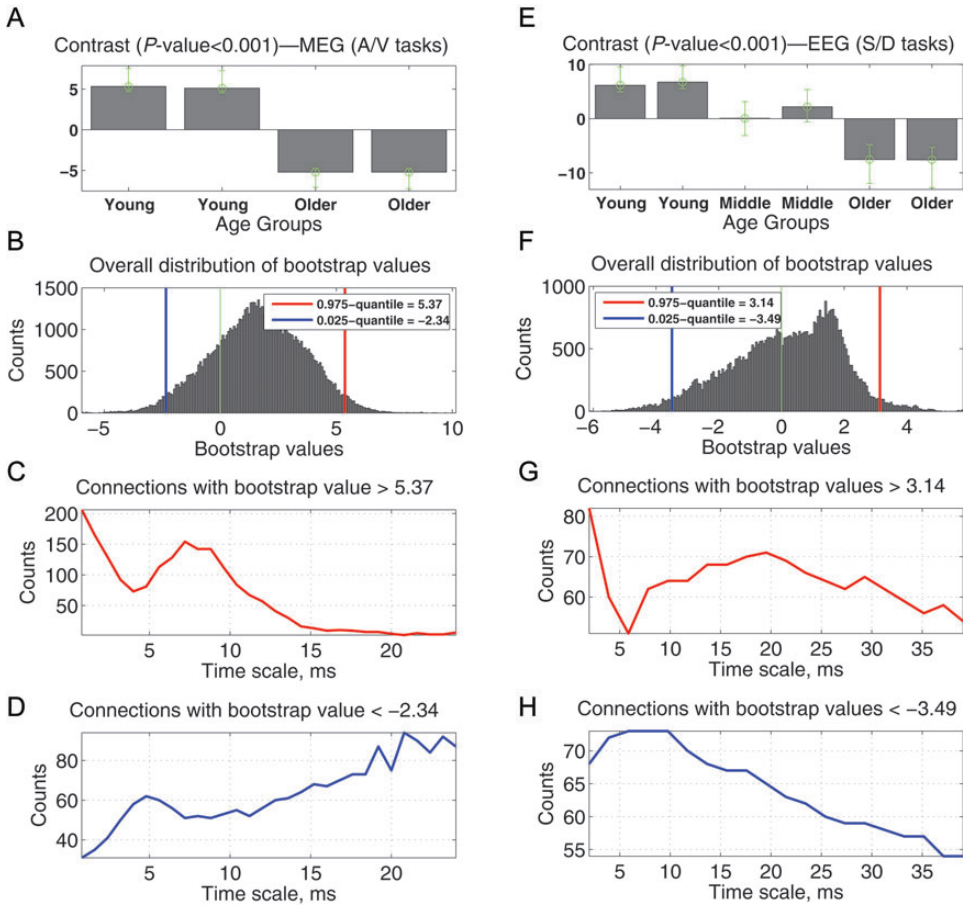

Figure 4. Age-related changes in distributed entropy: MEG (left) and EEG (right), from the PLS analysis. Panels (*A*) and (*E*) illustrate the data-driven contrasts. Expression of these trends is shown in (*B*) and (*G*) as the distributions of all the bootstrap ratio values for the distributed entropy between each pair of regional sources. The strengths of the effects related to a decrease (*C*,*G*) and increase (*D*,*H*) in distributed entropy are plotted as the number of connections whose bootstrap ratio values belong to the corresponding 2.5% tails.

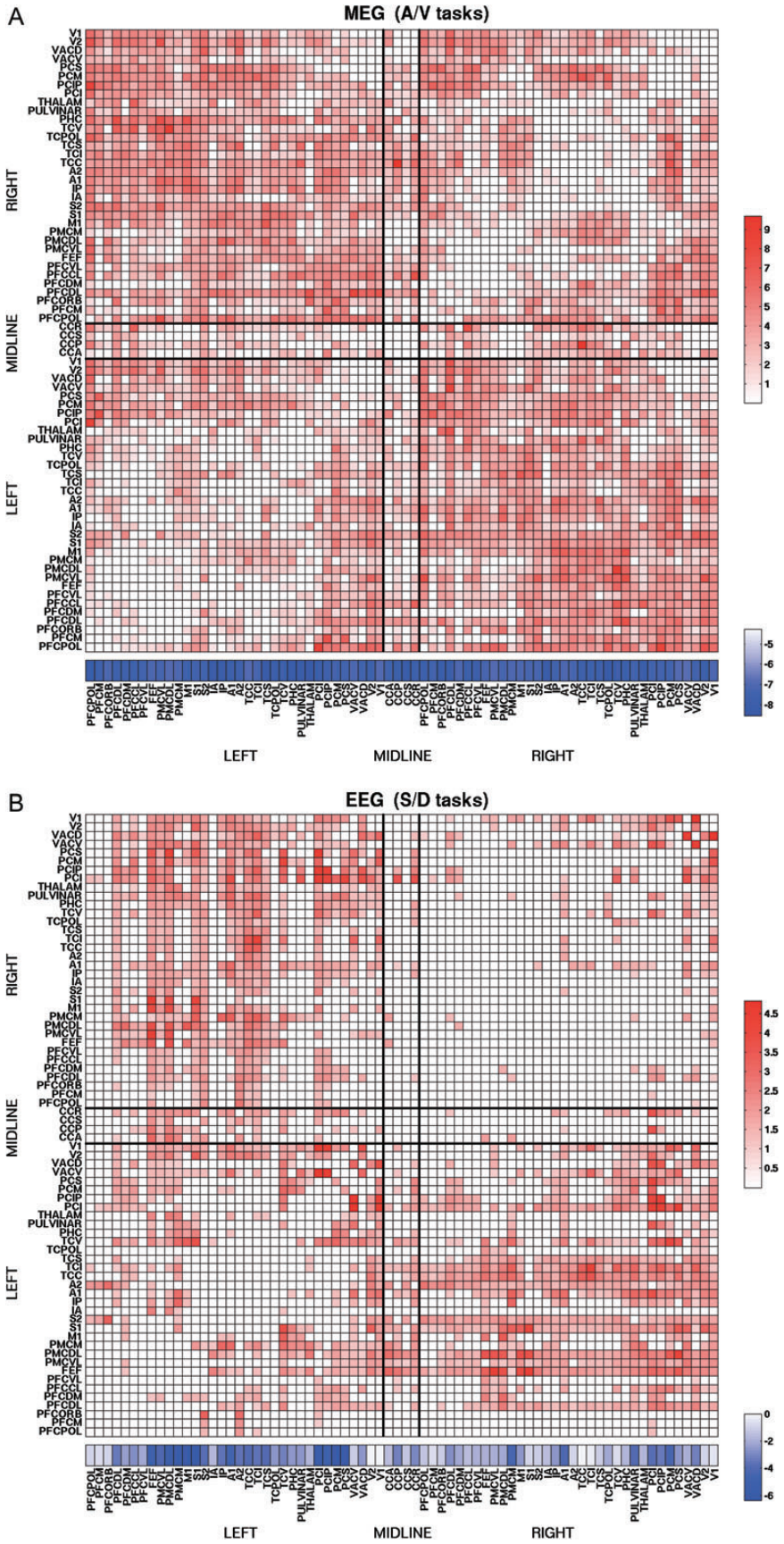

Figure 5. Matrix showing bootstrap ratios for pairwise age-related decreases in distributed entropy based on (*A*) MEG data; (*B*) EEG data. Plotted in the matrices, from the 7 ms timescale for MEG and 20 ms for EEG, are the connections associated with the bootstrap ratio values that are larger than one. The corresponding distribution of the bootstrap ratio values for local entropy across brain regions is shown below the matrix.

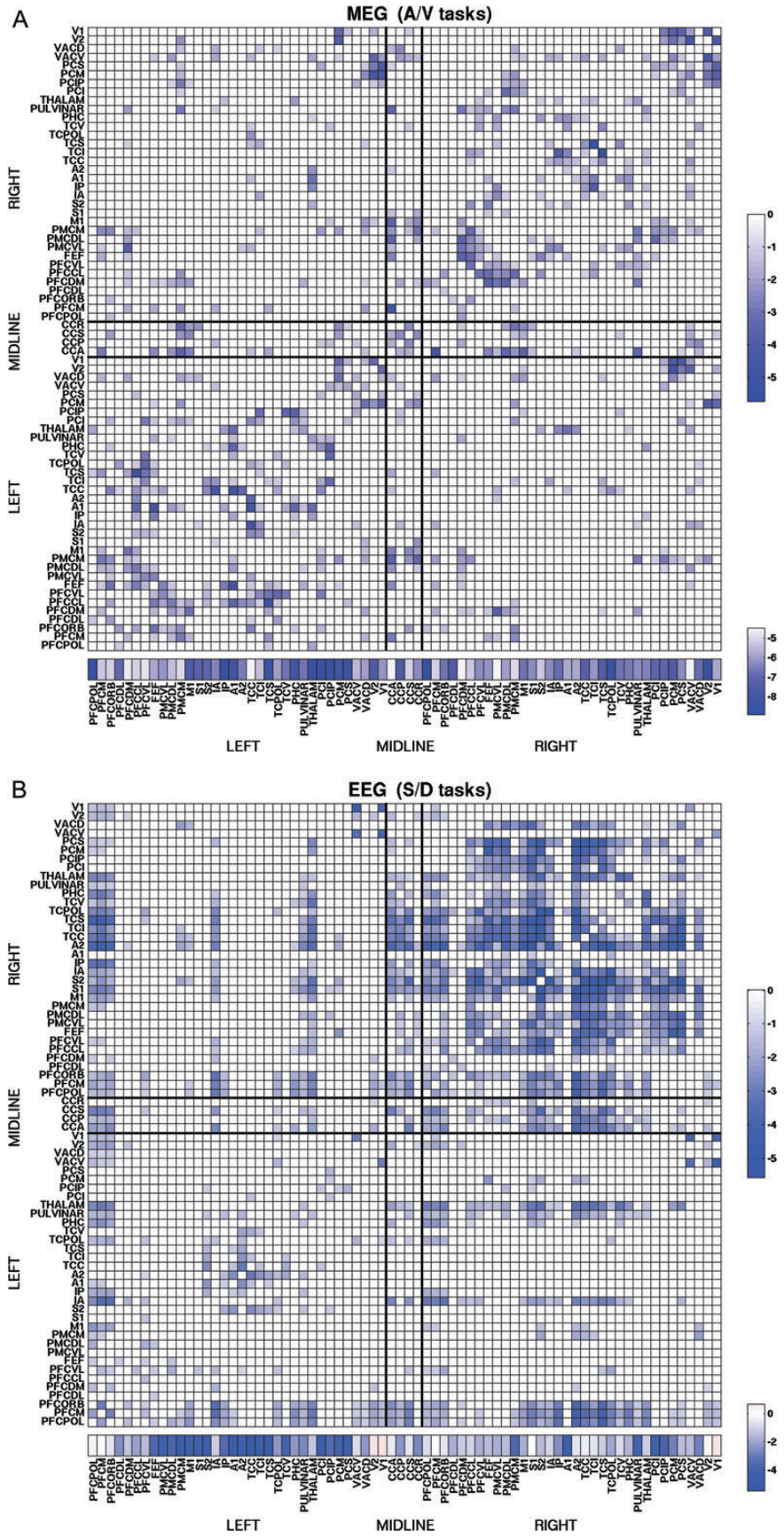

Figure 6. Matrix showing bootstrap ratios for pairwise age-related increases in distributed entropy based on (*A*) MEG data; (*B*) EEG data. Plotted in the matrices, from the 27 ms timescale for MEG and 8 ms for EEG, are the connections associated with the bootstrap ratio values that are larger than one. The corresponding distribution of the bootstrap ratio values for local entropy across brain regions is shown below the matrix.

Figure 5, the dominant effect in the pattern of age-related decreases in connectivity is represented by the communication between the hemispheres (right/left and left/right quadrants). In contrast to Figure 5, Figure 6 reveals that the increase in connectivity is supported mostly by the connections linking the brain areas that belong to the same hemispheres (left/left and right/right quadrants). It is worth noting that there is an overall agreement between MEG and EEG modalities with respect to the inter- and intra-hemispheric connections. It is noteworthy that in the case of EEG, however, the effects related to increased connectivity as a result of normal aging are expressed most strongly in the right hemisphere. We emphasize again that for both figures, we purposely chose a liberal statistical threshold for the plots to indicate that the pattern is not an artifact of an arbitrary threshold.

Discussion

Across two independent data sets, one using EEG and one MEG and each using different source reconstruction algorithms, we observed similar changes in brain signal variability, measured using MSE, with normal aging. As was hypothesized, these differences were dependent on the temporal scale of investigation. Finer timescales showed an increase with normal aging, whereas more coarse timescales showed a decrease in normal aging. The MSE results were then broken down further using the estimation of local and distributed entropy. The significance of the MSE findings can be appreciated in two different perspectives. First, there has been an emphasis in the neurophysiology literature on long-range correlations within time series as a reflection of the formation of associations and networks (Nunez 1989). Although it is likely the case that finer timescales reflect local dynamics, in this case reflecting neural populations, the more coarse timescales would reflect longer-range interactions with other populations. The observations in this paper suggest that with age, comes a shift from long-range connections (captured by coarse scales in MSE and distributed entropy estimates) to more local processing (captured at fine scales in MSE and local entropy estimates). This stands in a nice juxtaposition to the observations early in life that seemed to reflect an increase in long-range interactions and a concomitant decrease in local entropy (Vakorin et al. 2011). We found that in aging, this situation is reversed, suggesting that the interplay between integration and specialization can be described as a U-shaped function of age over the lifespan. We also observed a widespread increase in local entropy. This may suggest more functional independence for different brain areas in normal aging. There is correspondence between this idea and observations from graph theory metrics applied to functional connectivity in fMRI across young and old adults (Meunier et al. 2009). The essential finding from that study was that older adults on average had more modules than younger adults, with few that integrated spatially distant nodes. It is reasonable to link this finding with the current ones by suggesting that an increase in modularity would correspond to the observed increase in local entropy and potentially the concomitant decrease of distributed entropy.

An important observation from our study is that the age-related changes are temporally dependent. This is quite evident from the MSE analysis, where fine scales showed higher entropy and coarse scales showed lower entropy with age. In some respects, such temporal dependence could have been predicted from the work on spectral power changes in normal aging, in which low frequencies, in general, decrease in power whereas higher frequencies tend to increase (Dustman et al. 1993; Dustman et al. 1999), which was also observed in our data sets (see Supplementary Figures). Our MSE results mirror this. Moreover, the analysis of local and distributed entropy extend the interpretation by showing that local entropy, which is most highly correlated with fine scales in MSE, increases with age, and is mostly reflected in high frequency dynamics.

Although tempting to make a general statement that distributed entropy shows a complementary decrease in aging, the picture is not so simple. We do note that there are more decreases than increases in distributed entropy, but the decreases predominantly involve cross-hemispheric interactions. Studies of EEG coherence have also noted the reduction in interhemispheric functional connections with age (Duffy et al. 1996; Kikuchi et al. 2000). The observed decrease in distributed entropy seems to be consistent with previous studies, indicating that both the axonal and myelin integrity of the white matter is compromised in aging (Bartzokis et al. 2004; Head et al. 2004; Persson et al. 2006; Makris et al. 2007; Kennedy and Raz 2009; Seidler et al. 2010). In particular, a number of studies reported age-related deterioration of white-matter microstructure of corpus callosum (Doraiswamy et al. 1991; Sloane et al. 1999; Abe et al. 2002; Sullivan et al. 2010) that is in accordance with our finding indicating age-related decrease in distributed entropy between the hemispheres.

Conclusions

The intersection of studies in human neuroimaging from EEG and fMRI have emphasized that the brain operates at many different spatial and temporal scales, whereas theoretical expositions underscore the importance of the space–time structure as key to understanding processing capacity of brain networks (Jirsa and Kelso 2000; Deco et al. 2011). The essential points of this study revolve around spatiotemporal dependency as captured by measures of brain signal variability. In particular, we complete the picture of maturational changes in signal variability showing a general inverted-U trend from childhood to old age. There is an important caveat here—the nature of the latter part of this trend is critically dependent on temporal scale.

Supplementary Material

Supplementary material can be found at: http://www.cercor.oxfordjournals.org/.

Funding

This work was funded from grant 220020255 from the JS McDonnell Foundation and MT13623 from the Canadian Institutes for Health Research. Funding to pay the Open Access publication charges for this article was provided by grants 220020255 from the JS McDonnell Foundation and MT13623 from the Canadian Institutes for Health Research.

Notes

Conflict of Interest: The first two authors contributed equally to this paper.

References

Abe O, Aoki S, Hayashi N, Yamada H, Kunimatsu A, Mori H, Yoshikawa T, Okubo T, Ohtomo K. 2002. Normal aging in the central nervous system: quantitative MR diffusion-tensor analysis. Neurobiol Aging. 23:433–441.

Andrews-Hanna JR, Snyder AZ, Vincent JL, Lustig C, Head D, Raichle ME, Buckner RL. 2007. Disruption of large-scale brain systems in advanced aging. Neuron. 56:924–935.

Anokhin AP, Birbaumer N, Lutzenberger W, Nikolaev A, Vogel F. 1996. Age increases brain complexity. Electroencephalogr Clin Neurophysiol. 99:63–68.

Bartzokis G, Sultzer D, Lu PH, Nuechterlein KH, Mintz J, Cummings JL. 2004. Heterogeneous age-related breakdown of white matter structural integrity: implications for cortical "disconnection" in aging and Alzheimer's disease. Neurobiol Aging. 25:843–851.

Bhattacharya J, Edwards J, Mamelak AN, Schuman EM. 2005. Long-range temporal correlations in the spontaneous spiking of neurons in the hippocampal-amygdala complex of humans. Neurosci. 131:547–555.

Catarino A, Churches O, Baron-Cohen S, Andrade A, Ring H. 2011. Atypical EEG complexity in autism spectrum conditions: a multiscale entropy analysis. Clin Neurophysiol. 122:2375–2383.

Cheyne D, Bakhtazad L, Gaetz W. 2006. Spatiotemporal mapping of cortical activity accompanying voluntary movements using an event-related beamforming approach. Hum Brain Mapp. 27:213–229.

Costa M, Goldberger AL, Peng CK. 2002. Multiscale entropy analysis of complex physiologic time series. Phys Rev Lett. 89:068102.

Costa M, Goldberger AL, Peng CK. 2005. Multiscale entropy analysis of biological signals. Phys Rev E Stat Nonlin Soft Matter Phys. 71:021906.

Courchesne E, Chisum HJ, Townsend J, Cowles A, Covington J, Egaas B, Harwood M, Hinds S, Press GA. 2000. Normal brain development and aging: quantitative analysis at in vivo MR imaging in healthy volunteers. Radiology. 216:672–682.

Cox RW. 1996. AFNI: software for analysis and visualization of functional magnetic resonance neuroimages. Comput Biomed Res. 29:162–173.

Damoiseaux JS, Beckmann CF, Arigita EJ, Barkhof F, Scheltens P, Stam CJ, Smith SM, Rombouts SA. 2007. Reduced resting-state brain activity in the "default network" in normal aging. Cereb Cortex. 18:1856–1864.

Deco G, Jirsa VK, McIntosh AR. 2011. Emerging concepts for the dynamical organization of resting-state activity in the brain. Nat Rev Neurosci. 12:43–56.

Delorme A, Makeig S. 2004. EEGLAB: an open source toolbox for analysis of single-trial EEG dynamics including independent component analysis. J Neurosci Methods. 134:9–21.

Diaconescu AO, Alain C, McIntosh AR. 2011. The co-occurrence of multisensory facilitation and cross-modal conflict in the human brain. J. Neurophysiol. 106:2896–2909.

Diaconescu AO, Hasher L, McIntosh AR. 2012. Visual dominance and multisensory integration changes with age. Neuroimage. 65C:152–166.

Doraiswamy PM, Figiel GS, Husain MM, McDonald WM, Shah SA, Boyko OB, Ellinwood EH Jr., Krishnan KR. 1991. Aging of the human corpus callosum: magnetic resonance imaging in normal volunteers. J. Neuropsychiat Clin Neurosci. 3:392–397.

Duffy FH, McAnulty GB, Albert MS. 1996. Effects of age upon interhemispheric EEG coherence in normal adults. Neurobiol Aging. 17:587–599.

Dustman RE, Shearer DE, Emmerson RY. 1993. EEG and event-related potentials in normal aging. Prog Neurobiol. 41:369–401.

Dustman RE, Shearer DE, Emmerson RY. 1999. Life-span changes in EEG spectral amplitude, amplitude variability and mean frequency. Clin Neurophysiol. 110:1399–1409.

Efron B, Tibshirani RJ. 1993. An introduction to the bootstrap. New York: Chapman & Hall.

Efron B, Tibshirani R. 1986. Bootstrap methods for standard errors, confidence intervals and other measures of statistical accuracy. Stat. Sci. 1:54–77.

Gaal ZA, Boha R, Stam CJ, Molnar M. 2010. Age-dependent features of EEG-reactivity-Spectral, complexity, and network characteristics. Neurosci Lett. 479:79–84.

Garrett DD, Kovacevic N, McIntosh AR, Grady CL. 2011. The importance of being variable. J Neurosci. 31:4496–4503.

Garrett DD, Kovacevic N, McIntosh AR, Grady CL. 2013. The modulation of bold variability between cognitive states varies by age and processing speed. Cereb. Cortex. 23:684–693.

Good P. 2000. Permutation tests: a practical guide to resampling methods for testing hypotheses. New York: Springer.

Grady CL. 1998. Brain imaging and age-related changes in cognition. Exp Gerontol. 33:661–673.

Grady CL, McIntosh AR, Beig S, Keightley ML, Burian H, Black SE. 2003. Evidence from functional neuroimaging of a compensatory prefrontal network in Alzheimer's disease. J Neurosci. 23:986–993.

Grady CL, Protzner AB, Kovacevic N, Strother SC, Afshin-Pour B, Wojtowicz M, Anderson JA, Churchill N, McIntosh AR. 2010. A multivariate analysis of age-related differences in default mode and task-positive networks across multiple cognitive domains. Cereb.Cortex. 20:1432–1447.

Greenwood PM. 2000. The frontal aging hypothesis evaluated. J Int Neuropsychol Soc. 6:705–726.

Guttmann CR, Jolesz FA, Kikinis R, Killiany RJ, Moss MB, Sandor T, Albert MS. 1998. White matter changes with normal aging. Neurology. 50:972–978.

Head D, Buckner RL, Shimony JS, Williams LE, Akbudak E, Conturo TE, McAvoy M, Morris JC, Snyder AZ. 2004. Differential vulnerability of anterior white matter in nondemented aging with minimal acceleration in dementia of the Alzheimer type: evidence from diffusion tensor imaging. Cereb Cortex. 14:410–423.

Honey CJ, Kotter R, Breakspear M, Sporns O. 2007. Network structure of cerebral cortex shapes functional connectivity on multiple time scales. Proc Natl Acad Sci USA. 104:10240–5.

Jirsa VK, Kelso JA. 2000. Spatiotemporal pattern formation in neural systems with heterogeneous connection topologies. Phys Rev E Stat Phys Plasmas Fluids Relat Interdiscip Topics. 62:8462–8465.

Kaffashi F, Foglyano R, Wilson C, Loparo K. 2008. The effect of time delay on approximate & sample entropy calculations. Physica D. 237:3069–3074.

Kennedy KM, Raz N. 2009. Aging white matter and cognition: differential effects of regional variations in diffusion properties on memory, executive functions, and speed. Neuropsychologia. 47:916–927.

Kikuchi M, Wada Y, Koshino Y, Nanbu Y, Hashimoto T. 2000. Effect of normal aging upon interhemispheric EEG coherence: analysis during rest and photic stimulation. Clin Electroencephalogr. 31:170–174.

Kotter R, Wanke E. 2005. Mapping brains without coordinates. Philos Trans R Soc Lond B Biol Sci. 360:751–766.

Krishnan A, Williams LJ, McIntosh AR, Abdi H. 2011. Partial least squares (PLS) methods for neuroimaging: a tutorial and review. Neuroimage. 56:455–475.

Lippe S, Kovacevic N, McIntosh AR. 2009. Differential maturation of brain signal complexity in the human auditory and visual system. Front Hum Neurosci. 3:48.

Makris N, Papadimitriou GM, van der Kouwe A, Kennedy DN, Hodge SM, Dale AM, Benner T, Wald LL, Wu O, Tuch DS et al. 2007. Frontal connections and cognitive changes in normal aging rhesus monkeys: a DTI study. Neurobiol Aging. 28:1556–1567.

McIntosh AR, Bookstein FL, Haxby JV, Grady CL. 1996. Spatial pattern analysis of functional brain images using partial least squares. Neuroimage. 3:143–157.

McIntosh AR, Kovacevic N, Itier RJ. 2008. Increased brain signal variability accompanies lower behavioral variability in development. PLoS Comput Biol. 4:e1000106.

McIntosh AR, Lobaugh NJ. 2004. Partial least squares analysis of neuroimaging data: applications and advances. Neuroimage. 23(Suppl 1):S250–S263.

Meunier D, Achard S, Morcom A, Bullmore E. 2009. Age-related changes in modular organization of human brain functional networks. Neuroimage. 44:715–723.

Misic B, Mills T, Taylor MJ, McIntosh AR. 2010. Brain noise is task dependent and region specific. J Neurophysiol. 104: 2667–2676.
Nunez PL. 1989. Generation of human EEG by a combination of long and short range neocortical interactions. Brain Topogr. 1:199–215.
Park DC, Reuter-Lorenz P. 2009. The adaptive brain: aging and neurocognitive scaffolding. Ann. Rev. Psychol. 60:173–196.
Pascual-Marqui RD. 2002. Standardized low-resolution brain electromagnetic tomography (sLORETA): technical details. Methods Find Exp Clin Pharmacol. 24(Suppl D):5–12.
Persson J, Nyberg L, Lind J, Larsson A, Nilsson LG, Ingvar M, Buckner RL. 2006. Structure-function correlates of cognitive decline in aging. Cereb Cortex. 16:907–915.
Pierce TW, Kelly SP, Watson TD, Replogle D, King JS, Pribram KH. 2000. Age differences in dynamic measures of EEG. Brain Topog. 13:127–134.
Prichard D, Theiler J. 1995. Generalized redundancies for time series analysis. Physica D. 84:476–493.
Protzner AB, McIntosh AR. 2007. The interplay of stimulus modality and response latency in neural network organization for simple working memory tasks. J Neurosci. 27:3187–3197.
Protzner AB, Valiante TA, Kovacevic N, McCormick C, McAndrews MP. 2010. Hippocampal signal complexity in mesial temporal lobe epilepsy: a noisy brain is a healthy brain. Arch Ital Biol. 148:289–297.
Raz N, Rodrigue KM. 2006. Differential aging of the brain: patterns, cognitive correlates and modifiers. Neurosci Biobehav Rev. 30:730–748.
Seidler RD, Bernard JA, Burutolu TB, Fling BW, Gordon MT, Gwin JT, Kwak Y, Lipps DB. 2010. Motor control and aging: links to age-related brain structural, functional, and biochemical effects. Neurosci. Biobehav. Rev. 34:721–733.
Shannon CE. 1949. The Mathematical Theory of Communication. Urbana, Illinois: University of Illinois Press.
Silverman BW. 1986. Density estimation for statistics and data analysis. London: Chapman Hall.
Sloane JA, Hollander W, Moss MB, Rosene DL, Abraham CR. 1999. Increased microglial activation and protein nitration in white matter of the aging monkey. Neurobiol Aging. 20:395–405.
Snodgrass JG, Vanderwart M. 1980. A standardized set of 260 pictures: norms for name agreement, image agreement, familiarity and visual complexity. J. Exp. Psychol.: Hum. Learn. Mem. 6:174–215.
Sporns O, Tononi G, Edelman GM. 2000b. Connectivity and complexity: the relationship between neuroanatomy and brain dynamics. Neural Netw. 13:909–922.
Sporns O, Tononi G, Edelman GM. 2000a. Theoretical neuroanatomy: relating anatomical and functional connectivity in graphs and cortical connection matrices. Cereb Cortex. 10:127–141.
Srinivasan R, Nunez PL, Silberstein RB. 1998. Spatial filtering and neocortical dynamics: estimates of EEG coherence. IEEE Trans Biomed Eng. 45:814–826.
Sullivan EV, Rohlfing T, Pfefferbaum A. 2010. Longitudinal study of callosal microstructure in the normal adult aging brain using quantitative DTI fiber tracking. Develop Neuropsychol. 35: 233–256.
Tadel F, Baillet S, Mosher JC, Pantazis D, Leahy RM. 2011. Brainstorm: a user-friendly application for MEG/EEG analysis. Comput Intell Neurosci. 2011:879716.
Takahashi T, Cho RY, Murata T, Mizuno T, Kikuchi M, Mizukami K, Kosaka H, Takahashi K, Wada Y. 2009. Age-related variation in EEG complexity to photic stimulation: a multiscale entropy analysis. Clin Neurophysiol. 120:476–483.
Tononi G, Sporns O, Edelman GM. 1994. A measure of brain complexity: relating functional segregation and integration in the nervous system. Proc Natl Acad Sci USA. 91:5033–5037.
Vakorin VA, Lippe S, McIntosh AR. 2011. Variability of brain signals processed locally transforms into higher connectivity with brain development. J Neurosci. 31:6405–6413.
Zhang Y. 1991. Complexity and 1/f noise: a phase space approach. J Phys I. 1:971–977.